

Shock wave propagation and dispersion in glow discharge plasmas

Sergey O. Macheret,^{a)} Yuri Z. Ionikh,^{b)} Naira V. Chernysheva,^{b)} Azer P. Yalin, Luigi Martinelli, and Richard B. Miles

Department of Mechanical and Aerospace Engineering, Princeton University, D-414 Engineering Quadrangle, Princeton, New Jersey 08544

(Received 2 August 2000; accepted 6 June 2001)

Spark-generated shock waves were studied in glow discharges in argon and argon–nitrogen mixtures. Ultraviolet filtered Rayleigh scattering was used to measure radial profiles of gas temperature, and the laser schlieren method was used to measure shock arrival times and axial density gradients. Time accurate, inviscid, axisymmetric fluid dynamics computations were run and results compared with the experiments. Our simulation show that changes in shock structure and velocity in weakly ionized gases are explained by classical gas dynamics, with the critical role of thermal and multi-dimensional effects (transverse gradients, shock curvature, etc.). A direct proof of the thermal mechanism was obtained by pulsing the discharge. With a sub-millisecond delay between starting the discharge and shock launch, plasma parameters reach their steady-state values, but the temperature is still low, laser schlieren signals are virtually identical to those without the discharge, differing dramatically from the signals in discharges with fully established temperature profiles. © 2001 American Institute of Physics. [DOI: 10.1063/1.1388204]

I. INTRODUCTION

Weakly ionized gases (plasmas) could potentially have an impact on high-speed aerodynamics. Using plasmas for shock wave control, drag reduction, vehicle steering, sonic boom attenuation, ignition of combustion in engines, and magnetohydrodynamic (MHD) power extraction and enthalpy by-pass is being actively discussed. Of course, fundamental issues have to be resolved prior to any practical applications.

The propagation of shock waves in weakly ionized plasmas was studied in Russia,^{1–11,15,16} and, later, in the U.S.^{12–14} Shock acceleration, broadening, and “splitting” was observed in various direct current (dc), radio frequency (RF), and pulsed discharges, in inert as well as molecular gases. Some researchers^{1–14} attributed experimental observations to various plasma-specific phenomena, from electric double layers to ion-acoustic waves to new long-range interactions or microscopic structure formed in gas discharges. However, other Russian researchers^{15,16} found that their data can be adequately explained by conventional thermal phenomena. Gas heating, temperature inhomogeneity, and vibrational relaxation were theoretically shown to result in “anomalous” behavior of shocks in gas discharges.^{17–19}

In Refs. 20 and 21, analysis of various physical mechanisms resulted in a conclusion that the “broadening,” “splitting,” and acceleration of shocks in gas discharges could hardly be explained by plasma-specific effects. This is due ultimately to the very low ionization fraction in the discharges, which leads to a small fraction of the total gas energy stored in ionized and excited states, to very inefficient

energy and momentum transfer from electrons and ions to the bulk neutral gas, and to very long times of these transfer processes.

In 1997, two research groups simultaneously and independently showed, based on inviscid computational fluid dynamics (CFD) modeling,^{22,23} that transverse and longitudinal temperature and density gradients present in gas discharges due to Joule heating can be responsible for the observed “anomalous” shock profiles. The inviscid modeling of Ref. 22, extended in Ref. 24, emphasized that transverse gradients result in the multi-dimensional nature of shock propagation, and that attempts to interpret the phenomena in one-dimensional terms can be misleading. For example, shock curvature could be misinterpreted as a “broadened” or “split” one-dimensional (1D) structure. The inviscid results were confirmed in Navier–Stokes computations.²⁵ Additionally, as demonstrated in Ref. 25, in the case of very weak shocks (with a Mach number very close to 1) or very long propagation distances (many meters) wall shear could also result in an apparent “splitting” of laser schlieren signals even in a cold gas.

In the present paper, we describe a combined experimental and computational effort to clarify mechanisms of shock propagation in weakly ionized plasmas. Experiments were done in a well-characterized positive column of glow discharge in Ar and Ar–N₂ mixtures. Shock velocity and structure was measured using the laser schlieren method, similar to experiments of Refs. 12–14. Since the temperature and its gradients could play a critical role in shock propagation, radial temperature profiles in our experiments were measured with filtered Rayleigh scattering. Axisymmetric CFD modeling gives a very good agreement with experimental data, thus proving that it is classical, but multi-dimensional, gas dynamics that can account for the “anomalous” effects.

^{a)} Author to whom correspondence should be addressed. Electronic mail: macheret@princeton.edu

^{b)} Permanent address: Institute of Physics, St.-Petersburg State University, St.-Petersburg, Russia.

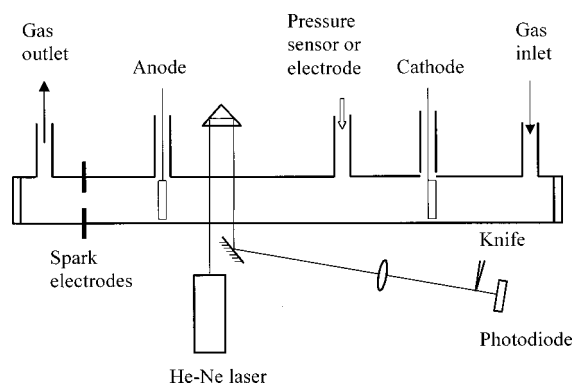


FIG. 1. Schematic of the experimental setup for studies of shock propagation in glow discharges.

In order to study shock propagation in weakly ionized plasma with very small or absent temperature gradients, pulsed discharge experiments were carried out. Those experiments prove again the thermal nature of shock propagation in gas discharges.

II. EXPERIMENTS ON SHOCK PROPAGATION IN STEADY-STATE GLOW DISCHARGES

A. Experimental setup and procedures

The experimental setup at Princeton University^{26,27} is basically similar to that of Refs. 12–14. The plasmas studied were created by a longitudinal continuous or pulsed glow discharge. The discharge tube, 3.8 cm i.d. and 120 cm full length, was made of quartz. Shock waves were generated by a spark discharge at the one end of the tube. The spark circuit parameters are capacitor 0.2 μF , voltage 15–20 kV. The capacitor discharge was controlled by a triggering spark gap. The shock wave entered the discharge through a narrow (2 mm wide and 0.1 mm thick) ring electrode made of stainless steel foil mounted adjacent to (almost flush with) the wall. The electrode nearest to the spark was always the anode, in order to prevent the incoming shock wave from passing by the hot cathode and through the cathode fall of the discharge. The cathode in all pulse and most steady-state experiments was identical in size and material to the anode. In some experimental runs, where shock profiles deep inside the plasma, far from the cathode, were studied, another cathode was used: a 25 mm diameter hollow cylinder with the axis perpendicular to the tube axis. This cathode was used only when it was far enough downstream of the shock and could not affect shock propagation. Both the cathode and anode could be placed at different locations in the tube, so that the distance between the spark and the anode could be 20 or 40 cm, and the length of discharge could be 20, 40, or 60 cm. The flexibility in changing the discharge length was used for measuring the electric field in the plasma (see below).

Similarly to Refs. 12–14, we used a laser schlieren method²⁸ for detecting the shock wave front (Fig. 1). A He–Ne laser beam crossed the discharge horizontally along the diameter and was then focused onto the plane of a knife by a lens ($f=50$ cm). The beam $1/e$ diameter was about 0.3 mm. A photodiode with a response time of 20 ns measured

the light intensity after the knife edge. The signal was recorded by a digital oscilloscope with 1 k Ω resistor at the input, and a time resolution ≈ 0.1 μs . In some measurements a miniature pressure sensor was also used.

To measure the instantaneous shock wave velocity we used an approach similar to that proposed in Ref. 29. After the laser beam crossed the discharge it was retro-reflected from a small 90° prism and passed through the discharge once more with the spatial offset and then focused onto the knife edge. This produced two closely separated schlieren signals of opposite signs. Shock wave velocity was found by dividing the distance between the two beam passages (12 to 21 mm) by the time gap between the schlieren signals. This method provided an accuracy of absolute velocity near 3 percent (≈ 10 m/s) and that of relative velocity about 0.5 percent (2 m/s).

Experiments were performed in an Ar–N₂ mixture (1% of N₂). The addition of nitrogen substantially improved the radial uniformity of the discharge. A pure argon discharge contracted at currents $i > 30$ –40 mA (for pressures $p \geq 30$ Torr). With nitrogen the discharge was not contracted at all conditions studied ($p \leq 100$ Torr, $i \leq 100$ mA). To prevent electrophoresis and the accumulation of impurities, the gas mixture was pumped through the discharge with a rate of 300 sccm, which corresponded to 5–10 cm/s linear speed in the tube. Control measurements with the gas flow turned off for a short time gave shock velocities and schlieren profiles identical to those with the flow on.

As was already mentioned, the flexibility in changing the discharge length allowed us to measure an electric field E in a positive column of the discharge (cathode voltage drop V_c could also be found in these measurements). For $p=30$ –50 Torr, $i=30$ –100 mA the E value was from 8 to 14 V/cm. Assuming a Bessel radial profile for gas temperature, we calculated the reduced electric field E/N (N is the gas number density) and electron number density n_e . Averaged over the tube cross section, these values are $E/N=1.2$ –1.4 Td, $n_e=(1.2$ –4) $\times 10^{10}$ cm⁻³ for the condition range mentioned above.

B. Measurements of temperature profiles

We have used ultraviolet filtered Rayleigh scattering (UV FRS)^{30,31} to measure temperature profiles of the discharges studied. A summary of these measurements is presented here. A narrow linewidth laser is used to illuminate the sample gas and the scattered light is imaged through a narrow band absorption filter onto a detector, as shown schematically in Fig. 2. The laser should be tunable so that it may be tuned within an absorption notch, and narrow linewidth so that the elastic background (due to windows, particulates, etc.) is narrow compared to the spectral width of an absorption notch. The amount of scattered light measured by the detector depends on the spectral overlap of the scattered light and the filter absorption profile. The filter offers very nearly 100% transmission outside of the absorption notches, yet is extremely optically thick (suppression modeled as 10⁵ and higher) within the absorption notches. The light scattered by the atoms and/or molecules in the flow is thermally and col-

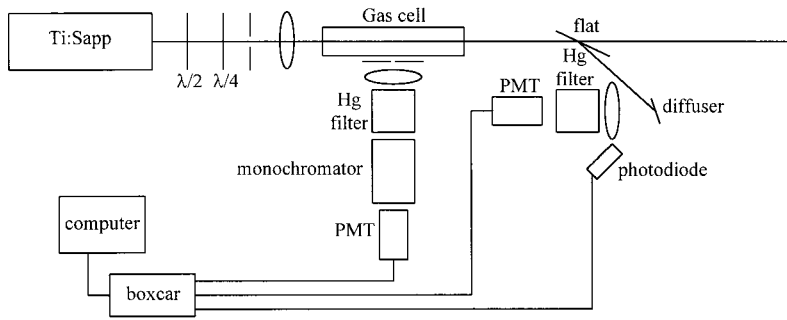


FIG. 2. Schematic diagram of experimental setup for UV FRS measurements of temperature profiles.

tionally broadened, and is therefore spectrally wider than the laser and background. When the laser is tuned to overlap an absorption notch, the filter serves to suppress the background while transmitting a large fraction of the light scattered from the flow. By an appropriate selection of filter conditions, and laser frequency, one may obtain very strong background suppression (greater than 10^5) while transmitting close to half the scattered light.

Depending on the conditions of a specific measurement, slightly different approaches may be used. In cases of constant (known) pressure we use a method which precludes the need for background subtraction. The approach is to ratio the FRS signal at a temperature to be measured, T_M , to the signal at a known temperature, T_{ref} . Both measurements are taken at the same frequency within an absorption notch so that any background is strongly suppressed in both cases. At constant pressure there is a one-to-one correspondence of temperature and density so that the measured ratio uniquely defines the unknown temperature T_M . The signal ratio is primarily determined by the density ratio, with a smaller opposing contribution from lineshape effects.

Modeling results for the present measurements are shown in Figs. 3 and 4. Figure 3 shows the modeled filter transmission profile and FRS signal levels as functions of

frequency. The filter has a length of 5 cm, a mercury vapor pressure of 0.0030 Torr, and a temperature of 315 K. In this spectral region, mercury has six absorption notches due to hyperfine splitting and different isotopic contributions. Figure 3 is a closer view of the highest frequency absorption notch—the one used in the current work. The nominal location of the lines is at 253.7 nm. The modeled FRS signal levels are for a scatterer of 50 Torr of argon at various temperatures. The Rayleigh scattering cross-section is not affected by the weak ionization and so the curves describe both argon gases and the plasmas used in these experiments. The signals are normalized to 300 K (by the ideal gas law) so that their relative magnitude scales as would be measured by a detector. In the absence of the filter the signal is linear with density (or $1/T$), while within the absorption features there is also a weaker effect from the variation of a scattering linewidth with temperature. From such modeling one may find the relationship between the experimentally measured FRS signal ratio,

$$\text{Ratio} = \text{FRS signal } (T = T_M) / \text{FRS signal } (T = T_{ref}),$$

and the unknown temperature T_M . Figure 4 is such a curve. In this case the unknown temperature, T_M , corresponds to

Modeled UV FRS signal levels for Argon, T=300,...,750 K

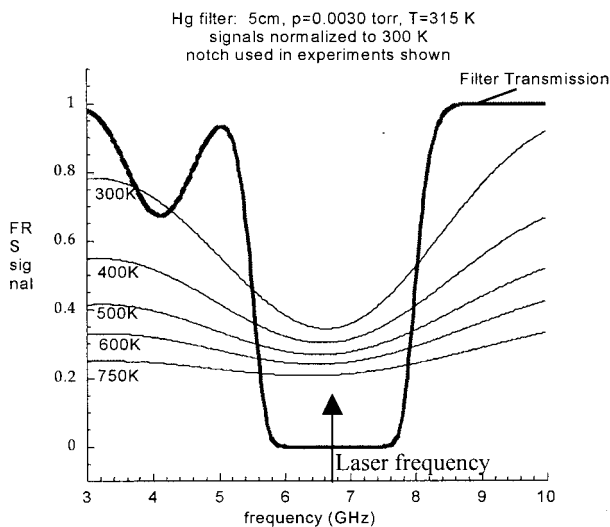


FIG. 3. Modeled FRS signal levels for argon at a range of temperatures. Mercury has several absorption notches in the 253.7 nm vicinity, however, Fig. 3 shows the experimentally used (high-frequency) notch.

Conversion Graph: Signal Ratio - Temperature

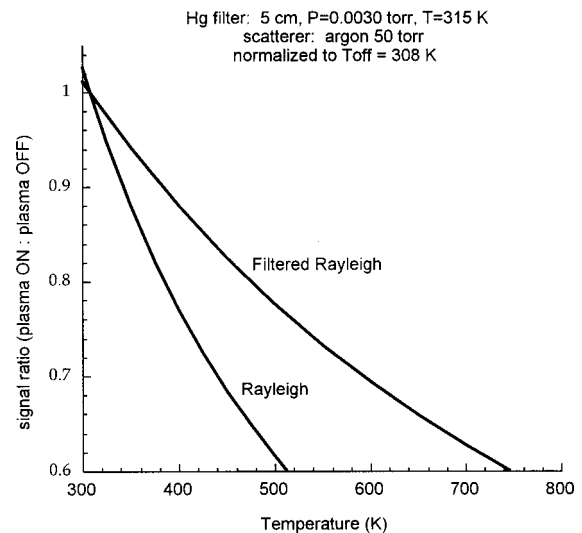


FIG. 4. Look-up graph used to convert signal ratio found with discharge ON/OFF to plasma temperature.

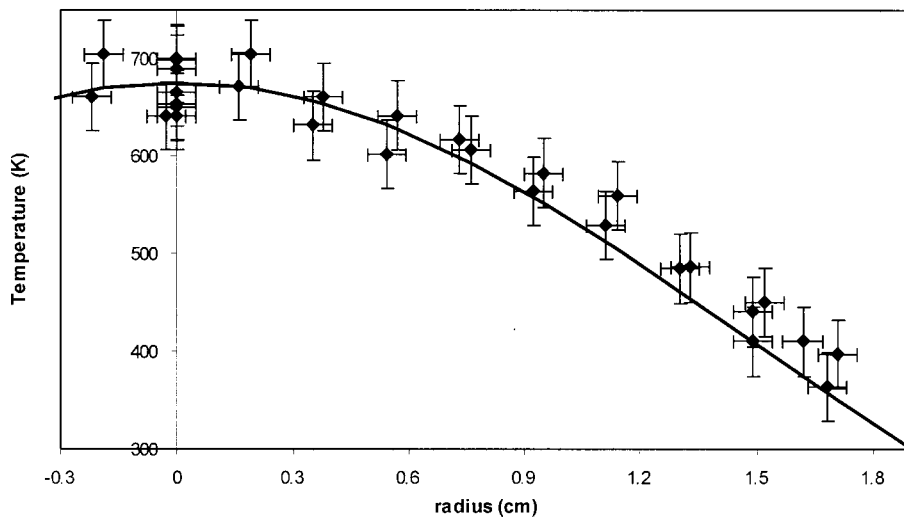
UV FRS Temperature Profile of Ar Plasma, $p=50$ torr, $i=20$ mA

FIG. 5. Radial temperature profile in an Ar glow discharge tube measured by UV filtered Rayleigh scattering. Pressure and electric current are indicated on the plot. Fitting curve—see Eq. (1).

the “plasma on” temperature while the reference temperature, T_{ref} , corresponds to the “plasma off” temperature—in this case $T_{\text{ref}}=308$ K.

The experimental configuration for FRS temperature measurements is illustrated in Fig. 2. A high power, tunable, narrow linewidth titanium sapphire laser³² was used as the excitation source. The frequency-tripled output was delivered to the plasma tube through several anti-reflection coated beam-shaping optics. For these experiments pulse energies of ~ 10 mJ in the ultraviolet (254 nm) were used. The beam passed through a quarter-wave plate to ensure the correct orientation of the linearly polarized beam, and through a half-wave plate to correct for the slight elliptical polarization introduced at the tube windows. Several irises were used to reduce stray light carried with a beam. A long focal length lens (~ 90 cm) was used to weakly focus the beam to a waist of ~ 200 microns at the sample volume. The sample volume was within the discharge tube and was defined by the laser beam waist and an iris located between the discharge tube and imaging lens ($f\# = 2.4$). The geometry was such that the sample volume had a length of about 1 mm. The scattered light was collected at a scattering angle of 90 degrees with the imaging lens and imaged through the mercury vapor filter. The filter had length 5 cm and had two temperature controllers yielding a vapor pressure of 0.003 Torr, and a filter temperature of 315 K. After the mercury filter, the light passed through a monochromator, which acted as a broad passband filter, while rejecting plasma luminosity and other colors of light from the laser. Finally, the scattered light signal was collected with a Hamamatsu R960 photomultiplier tube. After propagation through the discharge tube a quartz flat was used to pick off a fraction of the beam for power normalization as well as a frequency reference. The picked off beam illuminated a diffuser, and the elastically scattered light was detected through a second mercury filter (frequency reference), as well as measured by a photodiode (power reference). The latter two measurements used thin film interference filters (CORION G25-254-F) for spectral

filtering. The three signals were collected with a Stanford Research System boxcar onto a computer.

In plasma temperature profile measurements, a thermocouple was used to measure the wall temperature. Two 1-D translation stages were used to translate the discharge tube horizontally relative to the laser beam. Radial profiles along the horizontal axis were found by translating the discharge tube. Profiles were obtained in the argon plasma as well as the argon plus 1% nitrogen mixture, both at a pressure of 50 Torr, at several different values of electric current.

For the range of experimental conditions studied, $p=30$ –50 Torr, $i=30$ –100 mA, the steady-state centerline temperature range was found to be from 440 ± 30 K to 830 ± 70 K. Figure 5 shows the experimental profile of an argon plasma at pressure 50 Torr and current 20 mA. Figures 6 and 7 are experimental profiles of an argon + 1% nitrogen mixture at a pressure of 50 Torr, and currents of 10 and 40 mA, respectively. The experimental points are in good agreement with computation.³¹ We have plotted them here with fitted Gaussian curves:

$$\frac{T(r)}{T_w} = \frac{T_c}{T_w} \exp\left[-\ln \frac{T_c}{T_w} \cdot (r/R)^2\right], \quad (1)$$

where T_c and T_w are the centerline and wall temperature, respectively; r is the radial variable; and R is the tube radius.

III. RESULTS OF SHOCK PROPAGATION STUDIES IN STEADY-STATE DISCHARGES AND COMPARISON WITH CFD AXISYMMETRIC MODELING

In our earlier work,^{22,24} we performed a 2-D inviscid modeling of shock propagation through a discharge-heated gas and concluded that transverse gradient and multi-dimensionality play a crucial role in shock propagation in glow discharges, and that multi-peak laser schlieren signals are simply due to the shock curvature. For better comparison with experiments, in this work we developed an axisymmetric version of our code. The code solves the axisymmetric

UV FRS Temperature Profile of Ar + 1% N₂ Plasma, p=50 torr, i=10 mA

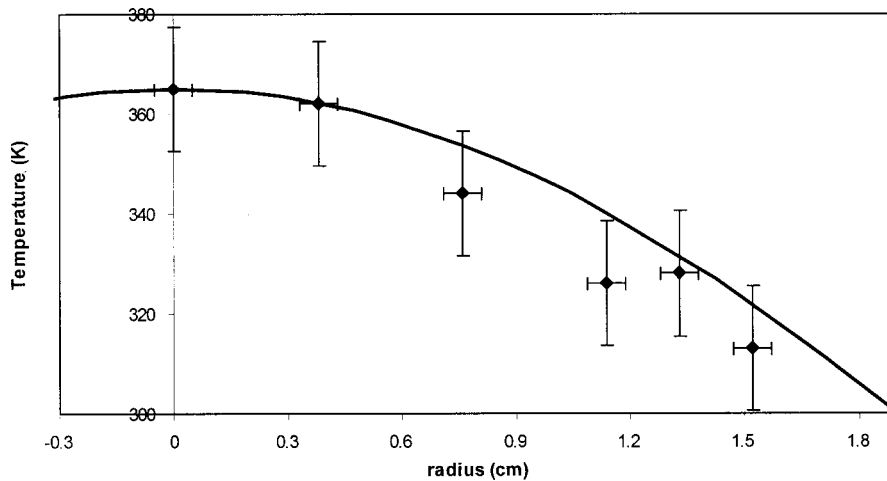


FIG. 6. Radial temperature profile in an Ar+1%N₂ glow discharge tube measured by UV filtered Rayleigh scattering. Pressure and electric current are indicated on the plot. Fitting curve—see Eq. (1).

conservative form of the Euler equations on unstructured, triangular, adaptive meshes. The flux balance and shock capturing were carried out by extending the Bhatnagar–Gross–Krook (BGK) solver developed and validated in Ref. 33 to axisymmetric problems. The grid adaption technique was identical to the one used for the two-dimensional code. The “driven” gas was initially at rest, and a shock wave of prescribed strength separated initially the “driven” gas from the “driver.” The state of the “driver” gas was specified according to the Rankine–Hugoniot conditions.

The subsequent development of the flow field was computed by solving time-dependent Euler equations in conservation form. Thus, no additional care was required to satisfy the Rankine–Hugoniot conditions, and the correct shock propagation and jump conditions across shocks and other discontinuities were captured by the solution.

As found in the earlier work,²⁴ to model shock structure on a 10 microsecond time scale, simple computations of a “piston-driven,” or “step” shock would suffice. This is due

to the fact that the initial spark-generated shock broadens so much in its 20–40 cm path to the discharge entrance or a measurement point that on the 5 mm distance (or 10 μ s time interval) from the shock front the shock is very close to a “step” shock.²⁴ This simplification, while being quite accurate, saved us from running extremely CPU-intensive full computations of the spark-generated pulse shocks. The plasma region between the infinitely thin electrodes was considered uniform along the tube axis (x), and to have a symmetric radial temperature profile described by the analytical fit (1) to the experimentally measured profile. Both the wall temperature and the gas temperature outside the discharge were set equal to room temperature. Thus, there was a sharp thermal diaphragm between the cold and hot regions. In the absence of diffusion (both physical and numerical) this diaphragm will remain fixed with respect to a quiescent gas until the incident shock impinges upon it. The initial position of the incident shock in the calculations reported here was one tube radius to the left from the boundary between the

UV FRS Temperature Profile of Ar + 1% N₂ Plasma, p=50 torr, i=40 mA

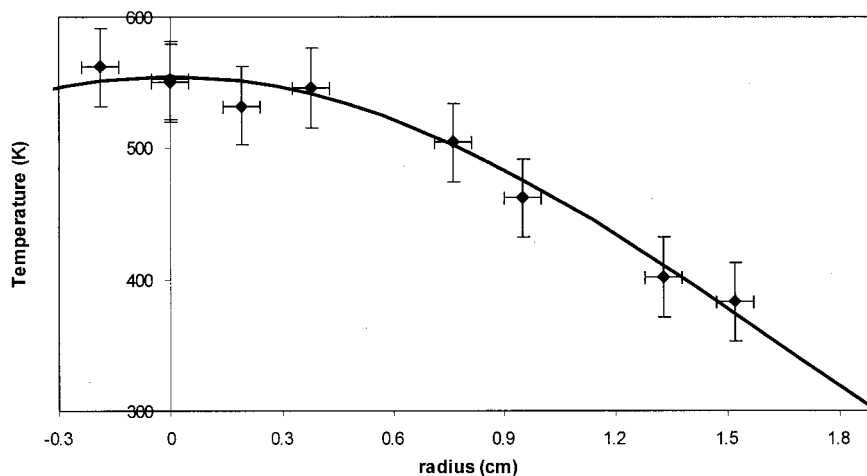


FIG. 7. Radial temperature profile in an Ar+1%N₂ glow discharge tube measured by UV filtered Rayleigh scattering. Pressure and electric current are indicated on the plot. Fitting curve—see Eq. (1).

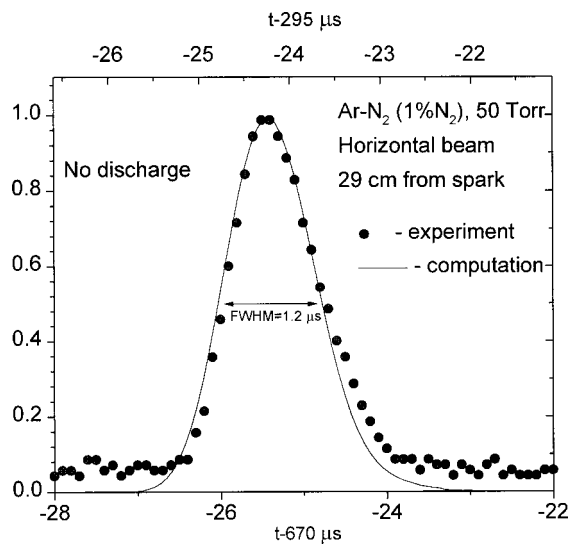


FIG. 8. Calibration of the “laser beam width” for CFD modeling against a laser schlieren signal with the discharge off. Note: experimental time t was measured from the moment of spark firing, while the computational time t was counted from the moment when the shock was located at a distance of one tube radius to the left of the discharge.

cold and the discharge-heated gases. Mach numbers of the incident shock were selected so as to give the shock velocity in the uniform room-temperature gas at a given location close to that measured experimentally with the discharge off.

For comparison with laser schlieren measurements, the density gradient integrated in the x direction across the nar-

row “laser beam” and averaged in the radial direction across the tube was computed. The “laser beam” width in the computations was adjusted once to match the experimentally determined width of the schlieren signal with the discharge off. The result of this calibration is shown in Fig. 8. As seen in the figure, computations reproduce the shape of the experimental peak very well.

Note that in the experiments time was measured from the moment of spark firing, while the computations started with the shock located at a distance of one tube radius to the left of the discharge region. Thus, computational time is shifted with respect to the experimental one by a constant. This is reflected in Figs. 8–11. For example, in Fig. 9, the experimental signals are plotted versus $(t-700 \mu\text{s})$, where t is the time from the spark firing, and the computational results are plotted against $(t-420 \mu\text{s})$, with the computational time t counted from the moment when the shock was located at a distance of one tube radius to the left of the discharge region. The constant shift of t obviously does not affect differential measurements or computations of shock velocity.

Figures 9–11 show measured and computed schlieren signals in pure argon (Fig. 9) and Ar+1%N₂ (Figs. 10 and 11). In each figure, upper plots correspond to the discharge-off case, while lower plots correspond to the discharge current of 20 mA (Fig. 9), and 10 and 40 mA in Figs. 10 and 11. Figures 10 and 11 differ in that the schlieren measurement point in Fig. 11 is about 11 cm downstream of that in Fig. 10. Measured and computed velocities of shock waves are shown near all the signals in Figs. 9–11.

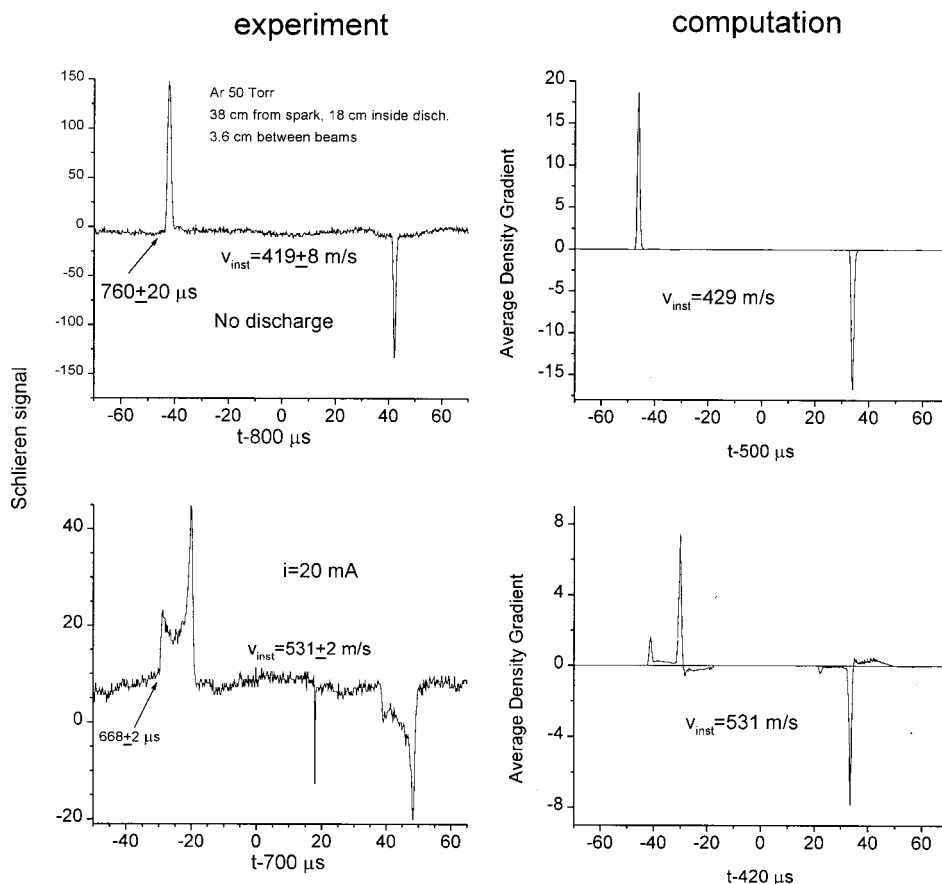


FIG. 9. Experimentally measured and simulated laser schlieren signals for shocks propagating in a glow discharge in pure Ar at 50 Torr. The discharge current is 20 mA. The first of the two laser beams is located 18 cm from the entrance to the discharge, and the spacing between the two beams is 3.6 cm. The experimentally measured and computed shock velocities are indicated in the figure. Note: experimental time t was measured from the moment of spark firing, while the computational time t was counted from the moment when the shock was located at a distance of one tube radius to the left of the discharge.

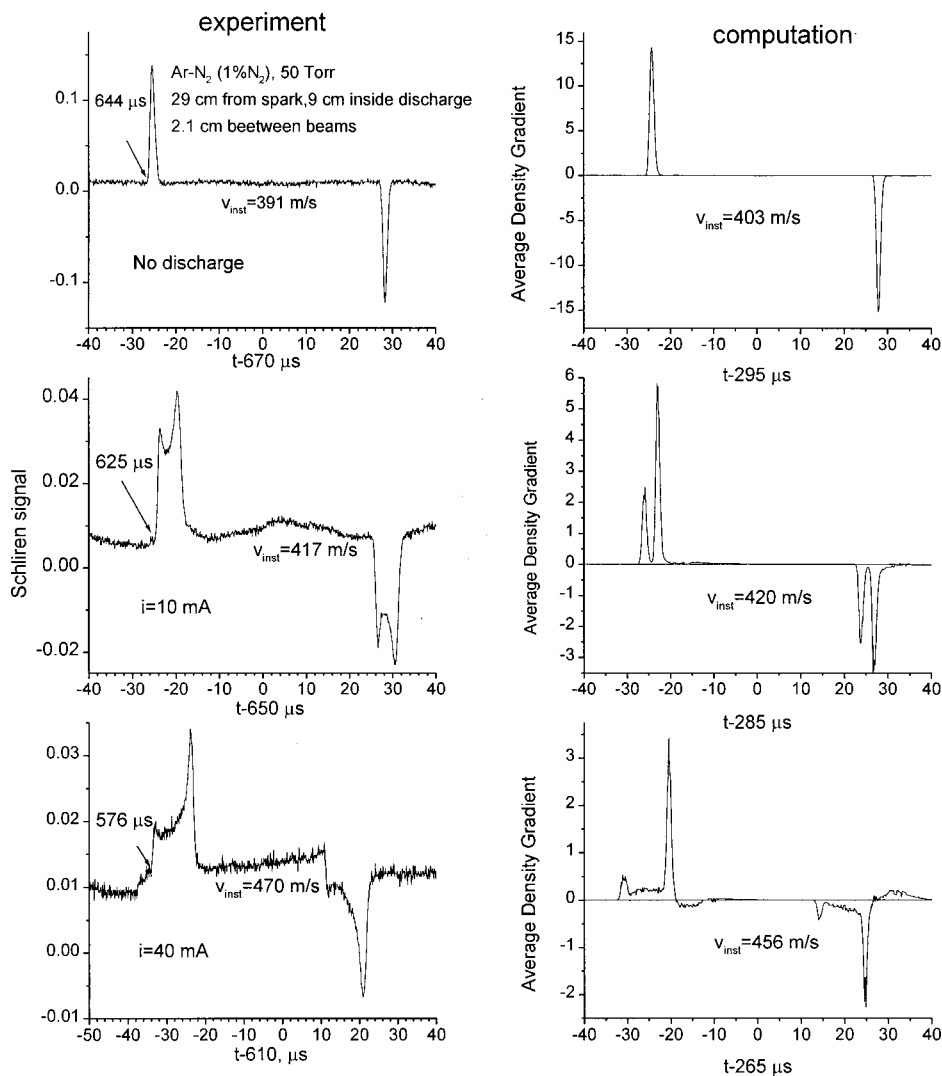


FIG. 10. Experimentally measured and simulated laser schlieren signals for shocks propagating in a glow discharge in Ar+1%N₂ at 50 Torr. The discharge current values are 10 mA and 40 mA. The first of the two laser beams is located 9 cm from the entrance to the discharge, and the spacing between the two beams is 2.1 cm. The experimentally measured and computed shock velocities are indicated in the figure. Note: experimental time t was measured from the moment of spark firing, while the computational time t was counted from the moment when the shock was located at a distance of one tube radius to the left of the discharge.

As seen in the figures, agreement between the computations and experiments, in both shock velocities and the two-peak signal shapes, is excellent. As discussed in Ref. 24, the two-peak structure of the laser schlieren signals is due to the curvature of the shock front in a region with transverse temperature gradient. This is illustrated in Figs. 12(a)–12(d), where lines of constant density are shown in four moments of time, as the shock propagated from the room-temperature gas into the plasma. Note that flow perturbations upstream of the moving shock, such as the distortion of the boundary between hot and cold regions seen in Figs. 12(c) and 12(d), do not affect shock propagation. The first peak in the schlieren signal comes from the portion of the shock that propagates through the hot centerline region. The high temperature and low density in this region result in both higher shock speed and lower intensity of the peak compared with those corresponding to colder near-wall regions. The portion of the shock moving through the cold near-wall region lags behind and produces a strong peak in the signal due to the high density near the wall. [Note that in Fig. 12(d), a well-resolved Mach stem is discernible near the wall.] The decrease in the schlieren signal following the first peak is due to the curvature of the shock. Indeed, the signal is propor-

tional to the axial component of the density gradient. Therefore, with the decrease of the shock angle with the tube axis from 90° to lower values [Fig. 12(d)], the signal weakens substantially.

Although in Figs. 9–11 the agreement between computed and experimentally measured parameters is excellent, it is not perfect. Specifically, computed shock velocities and distances between two peaks in schlieren signals agree very well with experimental values. On the other hand, computed height of both peaks in the signals relative to the signal strength between the peaks is higher than that in experiments. One of the principal uncertainties in computations is due to the use of Gaussian fit (1) to the experimentally measured temperature profile, especially since temperature measurements have their own errors. Next, neither experimental nor computational (the latter—due to the mesh size) resolution is perfect. Still another factor is the use of an inviscid model that disregards viscosity and heat conduction. According to the data of Ref. 34, kinematic viscosity of Ar at 50 Torr, 300 K, is $\nu=2.1$ cm²/s, and at 50 Torr, 600 K, it is $\nu=7.1$ cm²/s. Thermal diffusivity values are, of course, comparable with those of viscosity.³⁴ The total width of the signal (that is, the distance between the peaks) in Figs. 9–11 is

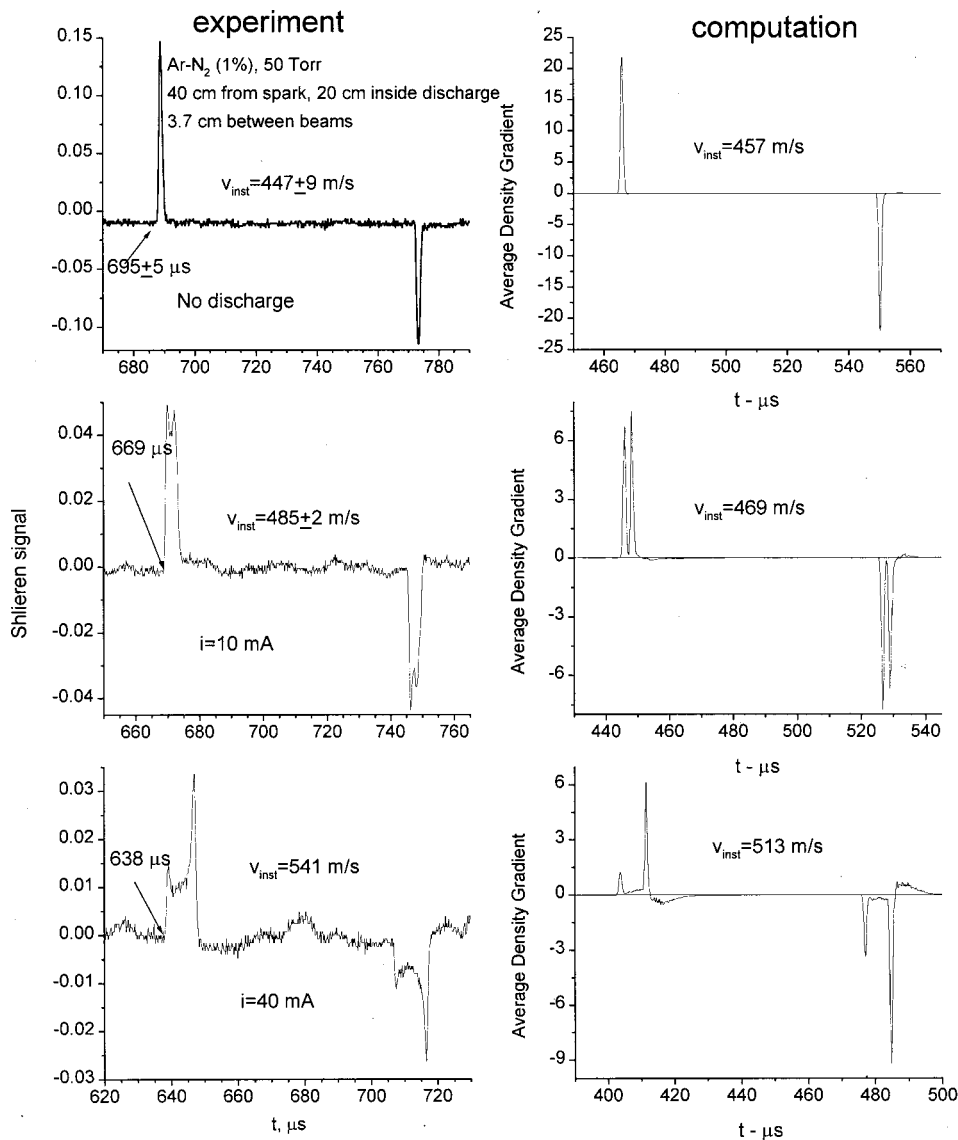


FIG. 11. Experimentally measured and simulated laser schlieren signals for shocks propagating in a glow discharge in Ar+1%N₂ at 50 Torr. The discharge current values are 10 mA and 40 mA. The first of the two laser beams is located 20 cm from the entrance to the discharge, and the spacing between the two beams is 3.7 cm. The experimentally measured and computed shock velocities are indicated in the figure. Note: experimental time t was measured from the moment of spark firing, while the computational time t was counted from the moment when the shock was located at a distance of one tube radius to the left of the discharge.

about $t=10 \mu s$. During this time, viscosity and heat conduction can smear velocity and density profiles on a length scale of $\delta \approx \sqrt{6\nu t} = 0.1-0.2$ mm. Since the width of each peak, converted into the length scale is about 0.5 mm, and the distance between the peaks—about 5 mm, viscosity and heat conduction cannot change the overall structure of the schlieren signals, which reaffirms the validity of inviscid modeling; however, some smearing of the signals can occur, helping to fill the “trough” between the peaks.

Note that since the linear velocity of the gas downstream of the shock is extremely low, 5–10 cm/s, boundary layer is virtually nonexistent prior to the shock arrival. Behind the shock, boundary layer thickness growth with distance x can be estimated, similar to the previous paragraph, as $\delta \approx \sqrt{6\nu t}$, where $t=x/u$, and u is the gas velocity behind the shock. On the time scale of 1–10 μs after the shock passage, the boundary layer will grow to only $\delta=0.03-0.09$ mm in our experimental conditions. Thus, the boundary layer is very thin in the vicinity of the shock and does not affect schlieren signals. As to the boundary layer farther upstream, it has no effect on the shock propagation.

For further quantitative comparison between computational and experimental results, Figs. 13 and 14 show the width of schlieren signals versus centerline temperature (Fig. 13) and the shock velocity versus average temperature in the discharge (Fig. 14), using the same set of shock propagation data. The average temperature was determined in a standard way:

$$T_{av} = \frac{\int_0^R T(r) \cdot 2\pi r dr}{\pi R^2}. \quad (2)$$

Again, Figs. 13 and 14 show excellent agreement between computations and experimental data. This provides a strong evidence of conventional, thermal mechanism of shock propagation in weakly ionized plasmas.

IV. EXPERIMENTS ON SHOCK PROPAGATION IN PULSED DISCHARGES

To distinguish between thermal and plasma-specific mechanisms of shock propagation, it would be desirable to eliminate temperature effects while maintaining plasma with

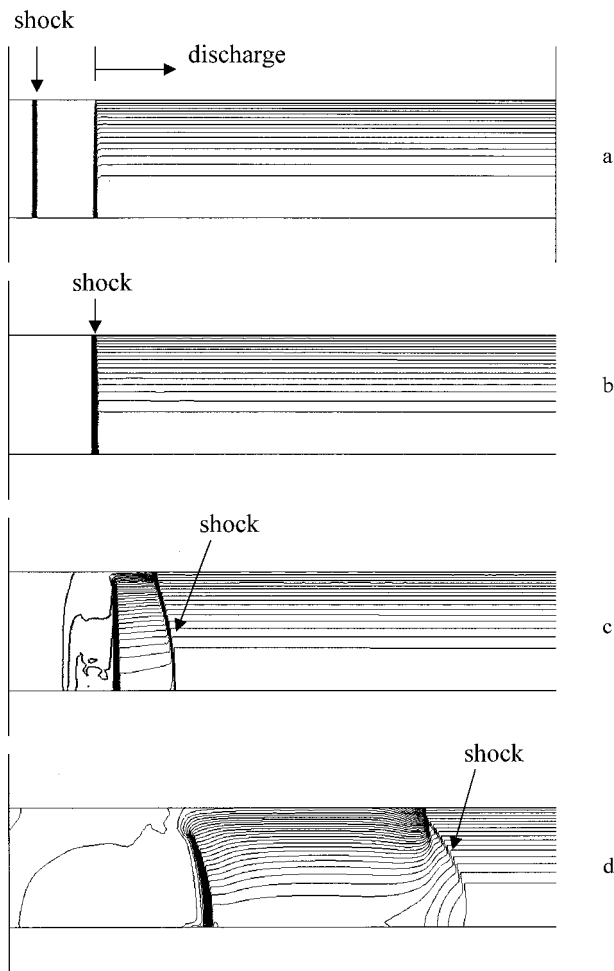


FIG. 12. Computed constant-density lines during shock propagation in a glow discharge tube (pure Ar, 50 Torr, 20 mA): (a) $t=21 \mu\text{s}$, prior to shock entry into the discharge; (b) $t=43 \mu\text{s}$, shock entering the discharge; (c) $t=60 \mu\text{s}$, shortly after the shock entered the discharge; (d) $t=123 \mu\text{s}$; the shock has penetrated deep inside the discharge. The computational time t was counted from the moment when the shock was located at a distance of one tube radius to the left of the discharge.

the same density of charged particles, electric field, etc. Unfortunately, a conventional steady-state discharge is a system where thermal effects are coupled with electric fields and electron density. However, in pulsed discharges, a relatively long time interval can exist when electron, ion, and excited molecule densities are quite high while the temperature is low. Indeed, gas heating and cooling occurs on time scale orders of magnitude longer than the time scale for ionization/recombination/excitation processes.³⁵

In this work, the pulsed mode of the discharge was produced by using a transistor switch in series with the discharge. The rise time for the current pulse was $20 \mu\text{s}$, and the pulse duration was about 0.5 ms. It was found that this time was insufficient to get a uniform discharge. In fact, when the discharge was turned on, undesirable transitional processes (for example, discharges on the wall of the tube) were observed. Therefore a weak pilot discharge with 1 mA current was maintained between pulses, which resulted in a fairly uniform volume pulsed discharge. Figure 15 shows the discharge pulse shape and the time dependence of discharge

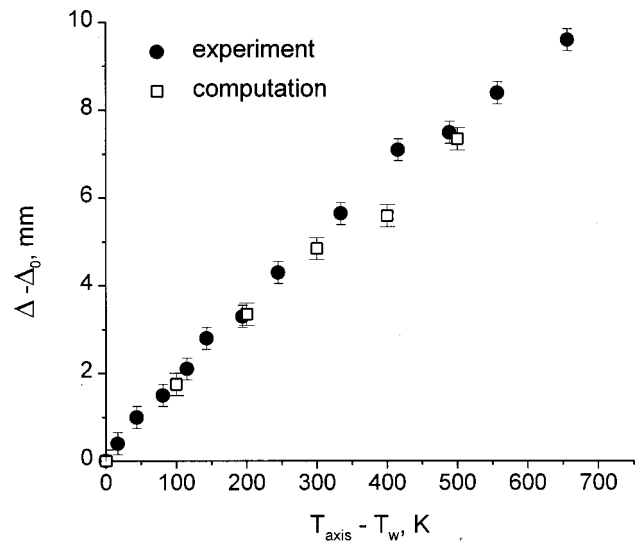


FIG. 13. The width of the schlieren signal in the discharge (Δ) minus the signal width with the discharge off (Δ_0) vs temperature difference between the axis and the wall, $T_{\text{axis}} - T_w$. Gas mixture Ar+0.16%N₂, pressure 50 Torr; 3 cm spark gap, 15 kV spark voltage; the first laser beam is 24.8 cm inside the discharge; spacing between the two beams is 2.9 cm.

integral emission (with no shock wave). Clearly, at times near to the middle of the pulse the emission reaches its steady-state value, similar to that of the continuous discharge. The initial peak of intensity is a result of the higher electric field arising in the discharge immediately after the transistor switch is opened (see below).

As shown in Figs. 16 and 17, for the pilot discharge a small acceleration, accompanied by some widening and weakening of the signal can be noticed, but the changes are very small compared to the higher-current continuous discharge. This is no surprise since the electron number density in the pilot discharge is $\approx 10^8 \text{ cm}^{-3}$ only and the measured axial gas temperature is less than 320 K.

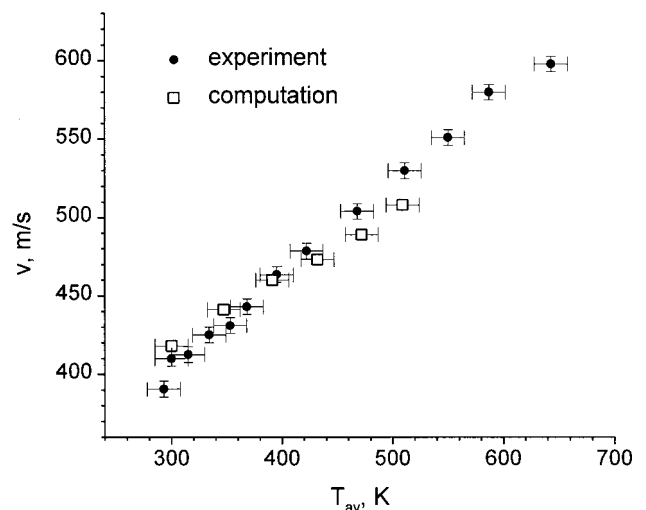


FIG. 14. Shock wave velocity vs average temperature [definition—see Eq. (2)] in the discharge. Gas mixture Ar+0.16%N₂, pressure 50 Torr; 3 cm spark gap, 15 kV spark voltage; the first laser beam is 24.8 cm inside the discharge; spacing between the two beams is 2.9 cm.

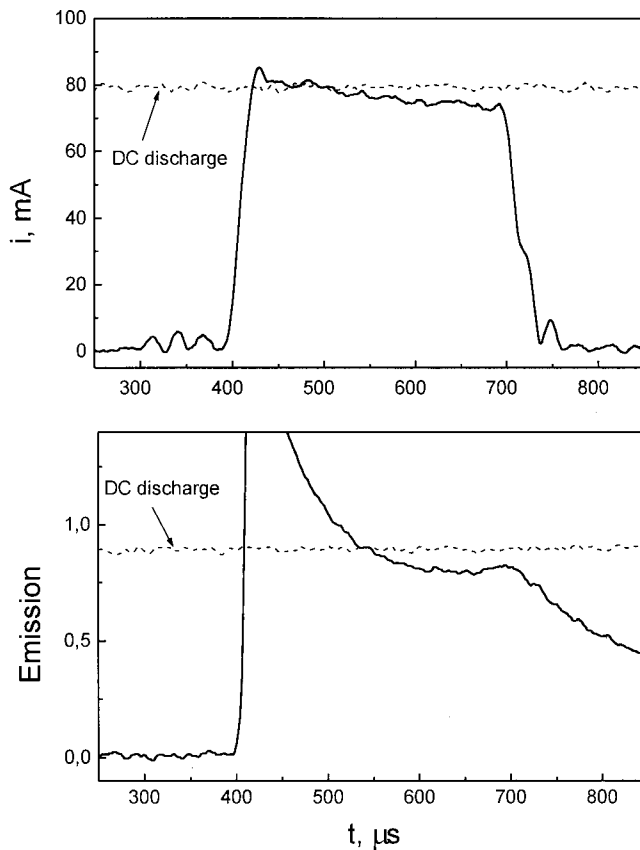


FIG. 15. Discharge current and integrated spectral emission vs time during the pulse.

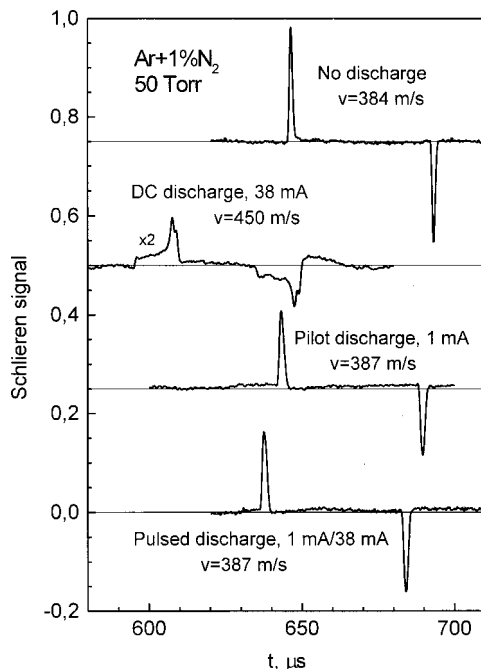


FIG. 16. Schlieren signals and shock velocities in a glow discharge in Ar+1%N₂ at 50 Torr: the discharge off; 38 mA continuous dc discharge, weak (1 mA) pilot discharge, and a pulsed discharge.

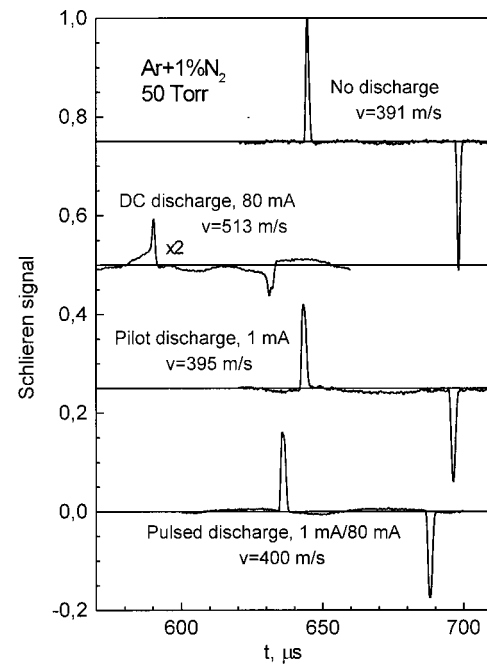


FIG. 17. Schlieren signals and shock velocities in a glow discharge in Ar+1%N₂ at 50 Torr: the discharge off; 80-mA continuous dc discharge, weak (1 mA) pilot discharge, and a pulsed discharge.

Much more important is that schlieren signal obtained from the pulsed discharge, as seen in Figs. 16 and 17, closely matches both no-discharge and pilot-discharge curves, and is very unlike the signal from the continuous discharge. After the transistor switch is turned on, the discharge current reaches its new steady-state value in $\approx 20 \mu\text{s}$. This value is almost the same as in continuous discharge. The electric field strength E in the pulse could be found by subtracting cathode drop V_c and voltage drop across the ballast resistor from the power supply voltage. The E values were found to be somewhat larger than in the continuous discharge, but the E/N values are almost identical. Thus, the electron number densities and mean electron energies (electron temperatures) should be very close to those in the continuous discharge. This is confirmed by the behavior of the discharge emission (Fig. 15). It reaches its steady-state value that is very close to that of the continuous discharge. An initial overshoot is related to the over voltage applied to the discharge in the transition period ($\sim 20 \mu\text{s}$) from small to large current. Higher E/N values in this interval result in efficient excitation of atoms and molecules, including those with radiative lifetime $\sim 1-10 \mu\text{s}$ (e.g., intensive bands of the first positive system of the N₂ molecule).

The increase in gas temperature, ΔT , during the pulse for the pulse duration τ_p may be calculated from the simple balance equation $iE\tau_p = c_p m_l \Delta T$, where c_p is the specific heat, and m_l is a mass of gas per unit length. Here we ignore heat losses because the pulse duration is a factor of 100 less than the characteristic time for thermal conductivity. For the conditions of Fig. 16, this equation gives $\Delta T = 0.4 \text{ K} - 0.6 \text{ K}$. Thus, the pulsed discharge has electron component parameters (E/N , n_e , T_e) the same as in the continuous discharge, but the gas temperature is the same as in the pilot discharge,

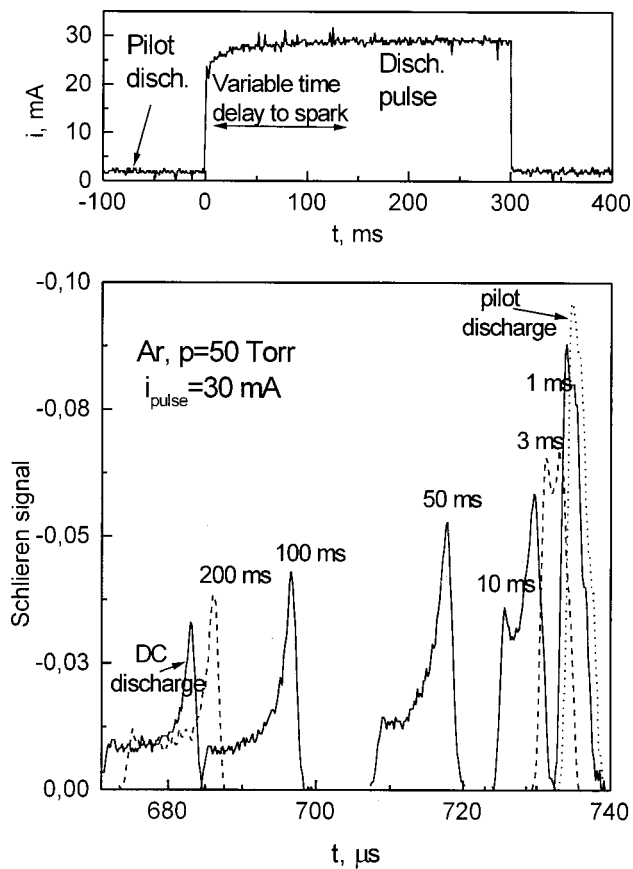


FIG. 18. Evolution of the schlieren signal at a fixed location inside the discharge with a time delay between the beginning of the discharge and the shock launch.

that is, close to room temperature. Comparing the three schlieren curves of Fig. 16 (and, similarly, those of Fig. 17) definitely shows that changing the electron density by two orders of magnitude does not affect shock wave propagation, while changing gas temperature from $T_g \approx 320$ K to $T_g \approx 500$ – 600 K (from the pilot or pulsed discharge to the continuous discharge) affects the shock dramatically. This result may be considered as a strong evidence of thermal mechanism of shock wave–plasma interaction.

To further illustrate the role of heating in shock dynamics, Fig. 18 shows schlieren signals taken with a time delay between turning the discharge on and launching the shock ranging from 1 ms to 200 ms. The 1-ms-delay signal is very close to that in the pilot discharge, while the 200-ms-delay signal is close to that in the continuous discharge. It takes tens and hundreds of milliseconds of the discharge existence for the signal to get close to its steady-state shape. The same point is also illustrated in Fig. 19, showing measured shock speed and schlieren signal width approaching their dc discharge values as the discharge is allowed to exist longer. Only gas heating in the discharge takes that long; ionization and excitation processes are many orders of magnitude faster.

As the discharge is turned off, one would expect thermal effects to persist for a long time, tens or even hundreds of milliseconds, when the recombination of a charged species and the quenching of excited states will be long since com-

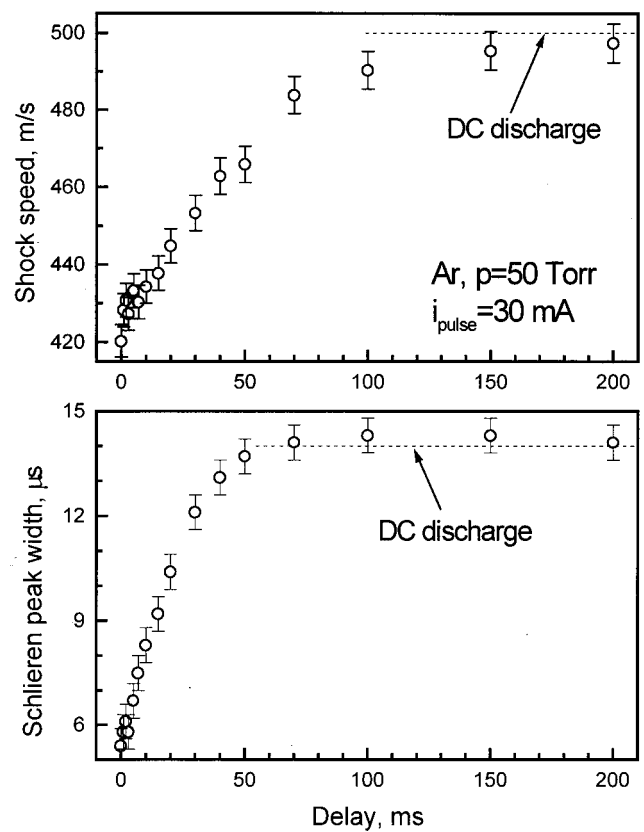


FIG. 19. Evolution of shock velocity and the width of the schlieren signal at a fixed location inside the discharge with time delay between the beginning of the discharge and the shock launch.

plete. Indeed, this persistence is clearly seen in Figs. 20 and 21, again supporting the thermal mechanism of shock–plasma interaction.

It should be noted that vibrational temperature, or populations of vibrational states, of nitrogen molecules, could be another parameter (apart from the gas temperature) that is quite different in pulsed and continuous discharges. The vibrational relaxation characteristic time is 1–2 orders of magnitude longer than the pulse duration, so the vibrational temperature in the pulsed discharge must be almost the same as in the pilot (1 mA) discharge.

To clarify the role of vibrational relaxation, shock wave propagation through pure argon discharge was also studied at low currents where contraction did not occur. In Fig. 22 schlieren signals for the two gases (Ar and Ar+1%N₂) are compared. The main features of schlieren signals for both cases are similar. For a more detailed comparison, one has to take into account that the addition of even 0.1%–1% of nitrogen to argon dramatically changes the electron drift velocity for the same E/N .³⁶ Another important factor found in our experiments is that the values of E/N in Ar+1%N₂ are substantially lower than those in pure Ar. Since E/N in the positive column is determined by the local ionization balance,³⁵ ionization, and/or recombination rates must be affected by the addition of nitrogen. The exact mechanism of the decrease in E/N with nitrogen addition is not clear at this time, and, being outside the immediate goal of this work, can be investigated in the future. One possible explanation is that

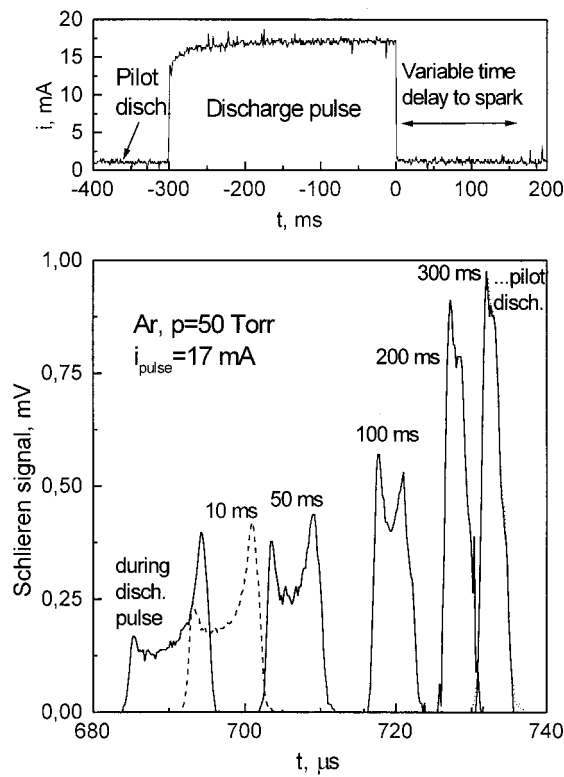


FIG. 20. Evolution of the schlieren signal at a fixed location inside the discharge with a time delay between the end of the discharge pulse and the shock launch.

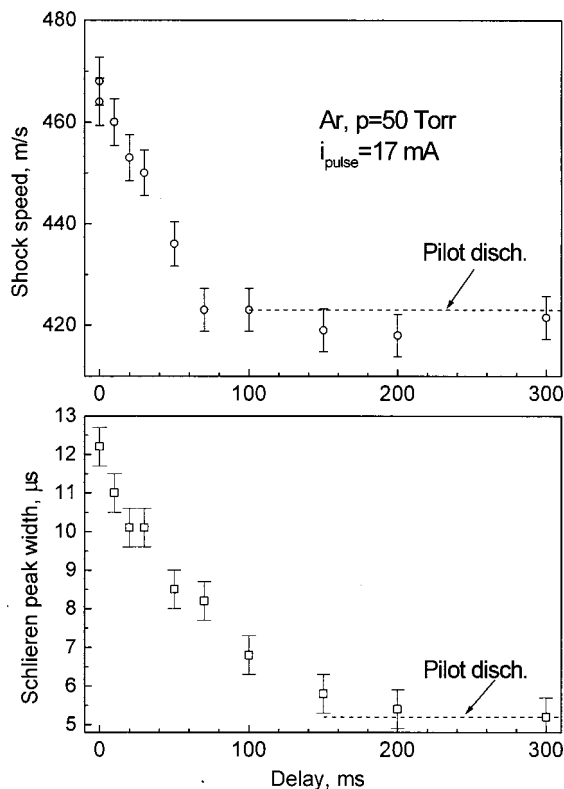


FIG. 21. Evolution of shock velocity and the width of the schlieren signal at a fixed location inside the discharge with time delay between the end of the discharge pulse and the shock launch.

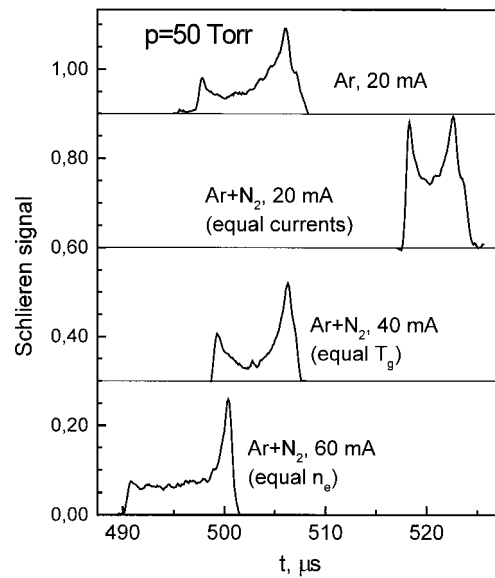


FIG. 22. A comparison of shock schlieren signals at a fixed location in Ar and Ar+1%N₂ discharges at 50 Torr and various values of the electric current.

metastables, such as N₂(³Σ), and vibrationally excited nitrogen molecules enhance the ionization. In any case, the reduction in E/N is an experimental fact, and it results in a lower gas temperature in Ar+1%N₂ even at the same current as in pure Ar (see, for example, Figs. 5 and 7). For a meaningful comparison of shock propagation data in Ar and Ar+N₂ mixtures, at least one of the parameters—electric current, electron number density, or gas temperature—should be the same in both cases. Data presented in Fig. 22 for Ar+1%N₂ mixture are shown at $i=20$ mA (the same as for pure argon), at 40 mA, where gas temperatures are close for both discharges, and at 60 mA, where electron densities are almost equal. It is evident that for the condition of almost-equal gas temperatures (40 mA) similarity of the patterns is the best. This eliminates unambiguously the vibrational relaxation effect and supplies more evidence of the thermal mechanism of shock dispersion.

V. CONCLUSIONS

Extensive experimental data on shock propagation in steady-state glow discharges in argon and argon–nitrogen mixtures were found to be in excellent agreement with high-accuracy axisymmetric CFD modeling. This provides compelling evidence that shock acceleration, attenuation, and “broadening” in weakly ionized plasmas can be explained by conventional gas dynamics, with multi-dimensionality (due to transverse temperature gradients) playing a critical role.

Experiments with pulsed discharges allowed us to separate thermal effects from those due to electric fields and charged particles. It turned out that gas heating is necessary for shock velocity and schlieren signal parameters to attain their steady-state values. This provides a direct proof of thermal mechanism of weakly ionized plasma effects on shock propagation.

ACKNOWLEDGMENT

This work was sponsored by the Air Force Office of Scientific Research.

- ¹G. I. Mishin, A. P. Bedin, N. I. Yushchenkova, G. E. Skvortsov, and A. P. Ryazin, "Anomalous relaxation and instability of shock waves in plasmas," *Sov. Phys. Tech. Phys.* **26**, 1363 (1981).
- ²A. I. Klimov, A. N. Koblov, G. I. Mishin, Yu. L. Serov, and I. P. Yavor, "Shock wave propagation in a glow discharge," *Sov. Tech. Phys. Lett.* **8**, 192 (1982).
- ³A. L. Klimov, A. N. Koblov, G. I. Mishin, Yu. L. Serov, K. V. Khodataev, and I. P. Yavor, "Shock wave propagation in a decaying plasma," *Sov. Tech. Phys. Lett.* **8**, 240 (1982).
- ⁴I. V. Basargin and G. I. Mishin, "Probe studies of shock waves in the plasma of a transverse glow discharge," *Sov. Tech. Phys. Lett.* **11**, 535 (1985).
- ⁵V. A. Gorshkov, A. I. Klimov, G. I. Mishin, A. B. Fedotov, and I. P. Yavor, "Behavior of electron density in a weakly ionized nonequilibrium plasma with a propagating shock wave," *Sov. Phys. Tech. Phys.* **32**, 1138 (1987).
- ⁶A. P. Ershov, S. V. Klislin, A. A. Kuzovnikov, S. E. Ponomareva, and Y. P. Pyt'ev, "Application of the reduction method to the microwave interferometry of shock waves in weakly ionized plasma," *Sov. Phys. Tech. Phys.* **34**, 936 (1989).
- ⁷I. V. Basargin and G. I. Mishin, "Precursor of shock wave in glow discharge plasma," *Sov. Tech. Phys. Lett.* **15**, 311 (1989).
- ⁸S. A. Bystrov, I. S. Zaslanko, Y. K. Mukoseev, and P. V. Shugaev, "Precursor ahead of a shock front in an RF discharge plasma," *Sov. Phys. Dokl.* **35**, 39 (1990).
- ⁹G. I. Mishin, A. I. Klimov, and A. Y. Gridin, "Measurements of the pressure and density in shock waves in a gas discharge plasma," *Sov. Tech. Phys. Lett.* **17**, 602 (1992).
- ¹⁰A. Y. Gridin, A. I. Klimov, and K. V. Khodataev, "Propagation of shock waves in a nonuniform transverse pulsed discharge," *High Temp.* **32**, 454 (1994).
- ¹¹A. Y. Gridin, A. I. Klimov, K. V. Khodataev, N. B. Shcherbak, and S. B. Shcherbak, "Two-dimensional simulation of shock wave propagation in a transverse pulse glow discharge with a heated cathode layer," *High Temp.* **32**, 755 (1994).
- ¹²B. N. Ganguly, P. Bletzinger, and A. Garscadden, "Shock wave damping and dispersion in nonequilibrium low pressure argon plasmas," *Phys. Lett. A* **230**, 218 (1997).
- ¹³B. N. Ganguly and P. Bletzinger, "Shock wave dispersion in nonequilibrium plasmas," Paper AIAA-96-4607, 1996.
- ¹⁴A. Garscadden, P. Bletzinger, and B. N. Ganguly, "Acoustic shock interaction in a positive column plasma," Paper AIAA-99-4973, 1999.
- ¹⁵N. V. Evtyukhin, A. D. Margolin, and V. M. Shmelev, "On the nature of shock wave acceleration in glow discharge plasma," *Sov. J. Chem. Phys.* **3**, 2080 (1986).
- ¹⁶P. A. Voinovich, A. P. Ershov, S. E. Ponomareva, and V. M. Shibkov, "Propagation of weak shock waves in plasma of longitudinal glow discharge in air," *High Temp.* **29**, 468 (1991).
- ¹⁷N. Babaeva, "On the structure of shock and blast waves in nonequilibrium plasma of gas discharge," *Khim. Fiz.* **12**, 357 (1993) (in Russian).
- ¹⁸N. Babaeva, A. Mnatsakanyan, and G. Naidis, "Simulation of shock wave propagation in a gas discharge developing in nitrogen," *High Temp.* **31**, 617 (1993).
- ¹⁹N. Babaeva and G. Naidis, "Simulation of shock wave propagation in gas discharge plasma regions," in *Proceedings of the Workshop Perspectives of MHD and Plasma Technologies in Aerospace Applications*, Moscow, 24–25 March 1999, p. 108.
- ²⁰I. V. Adamovich, V. V. Subramaniam, J. W. Rich, and S. O. Macheret, "Shock wave propagation in weakly ionized plasmas," Paper AIAA-97-2499, 1997.
- ²¹I. V. Adamovich, V. V. Subramaniam, J. W. Rich, and S. O. Macheret, "Phenomenological analysis of shock-wave propagation in weakly ionized plasmas," *AIAA J.* **36**, 816 (1998).
- ²²S. O. Macheret, L. Martinelli, and R. B. Miles, "Shock propagation in weakly ionized plasmas: Mechanisms and key problems," *Proceedings of the 1st Weakly Ionized Gases Workshop*, U.S. Air Force Academy, 9–13 June 1997, pp. X-11–X-33.
- ²³W. F. Bailey and W. M. Hilbun, "Baseline of thermal effects on shock propagation in glow discharge," in *Ref. 22*, pp. GG3–GG18.
- ²⁴S. O. Macheret, L. Martinelli, and R. B. Miles, "Shock propagation and structure in non-uniform gases and plasmas," Paper AIAA-99-0598, 1999.
- ²⁵S. M. Aithal and V. V. Subramaniam, "On the characteristics of a spark generated shock wave," *Phys. Fluids* **12**, 924 (2000).
- ²⁶Y. Z. Ionikh, N. V. Chernysheva, A. V. Meshchanov, A. P. Yalin, and R. B. Miles, "Direct evidence for thermal mechanism of plasma influence on shock wave propagation," *Phys. Lett. A* **259**, 387 (1999).
- ²⁷S. O. Macheret, Y. Z. Ionikh, L. Martinelli, P. F. Barker, and R. B. Miles, "External control of plasmas for high-speed aerodynamics," Paper AIAA-99-4853, 1999.
- ²⁸J. H. Kiefer and R. W. Lutz, "Simple quantitative schlieren technique of the high sensitivity for shock tube densitometry," *Phys. Fluids* **8**, 1393 (1965).
- ²⁹J. A. Bander and G. Sanzone, "An improved laser-schlieren system for the measurement of shock-wave velocity," *Rev. Sci. Instrum.* **45**, 949 (1974).
- ³⁰A. P. Yalin and R. B. Miles, "Ultraviolet filtered Rayleigh scattering temperature measurements with a mercury filter," *Opt. Lett.* **24**, 590 (1999).
- ³¹A. P. Yalin, Y. Ionikh, and R. B. Miles, "Temperature measurements in glow discharges with ultraviolet filtered Rayleigh scattering," Paper AIAA-99-3431, 1999.
- ³²N. D. Finkelstein, W. R. Lempert, and R. B. Miles, "Mercury vapor filter technology and ultraviolet laser source for flowfield imaging," Paper AIAA-97-0157, 1997.
- ³³C. A. Kim, A. Jameson, L. Martinelli, and K. Xu, "An accurate LED-BGK solver in unstructured adaptive meshes," Paper AIAA 97-0328, 1997.
- ³⁴*Handbook of Physical Quantities*, edited by I. S. Grigor'ev and E. Z. Meilikhov (CRC Press, Boca Raton, FL, 1997), Chaps. 15 and 16.
- ³⁵Yu. P. Raizer, *Gas Discharge Physics* (Springer-Verlag, Berlin, 1991), Chaps. 4, 10, and 14.
- ³⁶S. C. Brown, *Basic Data of Plasma Physics* (MIT Press, Cambridge, MA, 1966), p. 94.